insertion of the 5.5 kb *Bam*HI fragment of λ phage into pSV01[27]) was linearized with *Kpn*I, treated with alkaline phosphatase (AP), and ligated to an excess of the biotinylated *Kpn*I fragment. The product (containing nicked ligation junctions owing to the absence of plasmid-contributed phosphates) was digested with *Cla*I and *Xho*I. The resulting purified 7.3 kb fragment, designated protoSM, has the structure *Cla*I:7.2 kb:nick:97 bp(biotin-modified):*Xho*I. The torque-bearing DNA segment is the 14.8 kb *Bam*HI:*Sal*I fragment of pPIA6[28]. The final construct (SM1) was generated in a four-way ligation of the fluorescein-modified fragment, protoSM, torque-bearing segment, and DIG-modified fragment. Full-length products were selected by sequential binding to anti-fluorescein- and anti-DIG-coated beads in the optical tweezers. SM1 (Fig. 1a) was used in all reported experiments, with the following exceptions: SM2 (identical except DIG-DNA section extended to 601 bp for added stability) was used for the run shown in Fig. 2. SM3 (torque-bearing segment replaced with the 8.4 kb *Bgl*II-*Sal*I fragment of pSV8; fluorescein-DNA section extended to 4 kb) was used for the force–torque analysis of the B–S transition (red data points in Fig. 4b).

Experimental assembly and data collection

Anti-fluorescein beads were incubated with DNA and introduced into the flow chamber. Anti-DIG beads were introduced via a separate channel, and a molecular tether was assembled by keeping an anti-DIG bead on the micropipette by suction, and 'fishing' near a DNA:anti-fluorescein bead held in the laser trap. The trapped bead was then released into flow, and a streptavidin-coated 'rotor' bead was trapped and brought to the vicinity of the biotinylated portion of the molecule, where it became attached laterally to the DNA (Supplementary Movie 1). The micropipette was rotated using a computer-controlled electric motor (LEGO Mindstorms) while the rotor bead was held fixed by flowing buffer at $\sim$0.5 mm s^{-1}.

All experiments were performed in 100 mM NaCl and 40 mM Tris-HCl (pH 8.2). EDTA was typically present at 1 mM; omission caused no perceptible changes. Ambient temperature (23 $\pm$ 1 °C) was recorded prior to each experiment for use in viscosity calculations. Drag was also corrected for hydrodynamic coupling with the outer beads[29]; correction factors for the different rotor diameters were 1.005 (400 nm), 1.01 (520 nm), 1.02 (760 nm) and 1.03 (920 nm). Video was digitized at 30 Hz unless otherwise indicated, and the instantaneous angle of the rotor was extracted from the x-position and brightness (indicative of focal depth) of the bead. Angular velocities were obtained by numerical differentiation of the cumulative bead angle over a 1 s (Fig. 3) or 2 s (Fig. 2) window. The extrapolated P $\rightarrow$ B velocity of 400 nm beads (open circle in Fig. 3a inset) was obtained by measuring the velocity at large negative twists and scaling by $\tau_{\mathrm{crit},+}/\tau_{\mathrm{crit},-}$, since P $\rightarrow$ B rotation was too fast to track. During data collection, constant tension was maintained using stage-based force feedback[11]. During the exceptionally long run shown in Fig. 2 inset, force feedback (45 pN) was inoperative (out of actuator range) prior to $t = 23$ min, but $F > 30$ pN throughout.

Phase diagram

In the 'zero-temperature' approximation, the five-state structural model[10] leads to force–torque coexistence lines with constant slopes $\delta F/\delta\tau = -\Delta\theta/\Delta x$, where $\Delta\theta$ and Δx are the changes in twist and extension, respectively, for a particular structural transition. The slopes of the boundaries shown (Fig. 4b) were taken from experimental measurements of $\Delta\theta/\Delta x$, and predict the trends of the force–torque measurements. The intercepts of the boundaries were varied to fit the data. No torque measurements were made at the S–L or S–P boundaries, so these predicted slopes remain to be confirmed.

Received 6 February; accepted 28 May 2003; doi:10.1038/nature01810.

1. Smith, S. B., Finzi, L. & Bustamante, C. Direct mechanical measurements of the elasticity of single DNA molecules by using magnetic beads. *Science* **258,** 1122–1126 (1992).
2. Strick, T. R., Allemand, J. F., Bensimon, D., Bensimon, A. & Croquette, V. The elasticity of a single supercoiled DNA molecule. *Science* **271,** 1835–1837 (1996).
3. Smith, S. B., Cui, Y. & Bustamante, C. Overstretching B-DNA: The elastic response of individual double-stranded and single-stranded DNA molecules. *Science* **271,** 795–799 (1996).
4. Bustamante, C., Marko, J. F., Siggia, E. D. & Smith, S. Entropic elasticity of lambda-phage DNA. *Science* **265,** 1599–1600 (1994).
5. Cluzel, P. *et al.* DNA: An extensible molecule. *Science* **271,** 792–794 (1996).
6. Allemand, J. F., Bensimon, D., Lavery, R. & Croquette, V. Stretched and overwound DNA forms a Pauling-like structure with exposed bases. *Proc. Natl Acad. Sci. USA* **95,** 14152–14157 (1998).
7. Leger, J. F. *et al.* Structural transitions of a twisted and stretched DNA molecule. *Phys. Rev. Lett.* **83,** 1066–1069 (1999).
8. Bustamante, C., Bryant, Z. & Smith, S. B. Ten years of tension: Single-molecule DNA mechanics. *Nature* **421,** 423–427 (2003).
9. Bouchiat, C. & Mezard, M. Elasticity model of a supercoiled DNA molecule. *Phys. Rev. Lett.* **80,** 1556–1559 (1998).
10. Sarkar, A., Leger, J. F., Chatenay, D. & Marko, J. F. Structural transitions in DNA driven by external force and torque. *Phys. Rev. E* **63,** 051903 (2001).
11. Smith, S. B., Cui, Y. & Bustamante, C. Optical-trap force transducer that operates by direct measurement of light momentum. *Methods Enzymol.* **361,** 134–162 (2003).
12. Strick, T. R., Bensimon, D. & Croquette, V. Micro-mechanical measurement of the torsional modulus of DNA. *Genetica* **106,** 57–62 (1999).
13. Selvin, P. R. *et al.* Torsional rigidity of positively and negatively supercoiled DNA. *Science* **255,** 82–85 (1992).
14. Millar, D. P., Robbins, R. J. & Zewail, A. H. Direct observation of the torsional dynamics of DNA and RNA by picosecond spectroscopy. *Proc. Natl Acad. Sci. USA* **77,** 5593–5597 (1980).
15. Heath, P. J., Clendenning, J. B., Fujimoto, B. S. & Schurr, J. M. Effect of bending strain on the torsion elastic constant of DNA. *J. Mol. Biol.* **260,** 718–730 (1996).
16. Horowitz, D. S. & Wang, J. C. Torsional rigidity of DNA and length dependence of the free energy of DNA supercoiling. *J. Mol. Biol.* **173,** 75–91 (1984).
17. Shore, D. & Baldwin, R. L. Energetics of DNA twisting. II. Topoisomer analysis. *J. Mol. Biol.* **170,** 983–1007 (1983).
18. Crothers, D. M., Drak, J., Kahn, J. D. & Levene, S. D. DNA bending, flexibility, and helical repeat by cyclization kinetics. *Methods Enzymol.* **212,** 3–29 (1992).
19. Vologodskii, A. V. & Marko, J. F. Extension of torsionally stressed DNA by external force. *Biophys. J.* **73,** 123–132 (1997).
20. Moroz, J. D. & Nelson, P. Entropic elasticity of twist-storing polymers. *Macromolecules* **31,** 6333–6347 (1998).
21. Yasuda, R., Miyata, H. & Kinosita, K. Jr Direct measurement of the torsional rigidity of single actin filaments. *J. Mol. Biol.* **263,** 227–236 (1996).
22. Williams, M. C., Rouzina, I. & Bloomfield, V. A. Thermodynamics of DNA interactions from single molecule stretching experiments. *Acc. Chem. Res.* **35,** 159–166 (2002).
23. Soong, R. K. *et al.* Powering an inorganic nanodevice with a biomolecular motor. *Science* **290,** 1555–1558 (2000).
24. Yasuda, R., Noji, H., Kinosita, K. Jr & Yoshida, M. F1-ATPase is a highly efficient molecular motor that rotates with discrete 120 degree steps. *Cell* **93,** 1117–1124 (1998).
25. Seeman, N. C. DNA in a material world. *Nature* **421,** 427–431 (2003).
26. Harada, Y. *et al.* Direct observation of DNA rotation during transcription by *Escherichia coli* RNA polymerase. *Nature* **409,** 113–115 (2001).
27. Wobbe, C. R., Dean, F., Weissbach, L. & Hurwitz, J. *In vitro* replication of duplex circular DNA containing the simian virus 40 DNA origin site. *Proc. Natl Acad. Sci. USA* **82,** 5710–5714 (1985).
28. Davenport, R. J., Wuite, G. J., Landick, R. & Bustamante, C. Single-molecule study of transcriptional pausing and arrest by *E. coli* RNA polymerase. *Science* **287,** 2497–2500 (2000).
29. Davis, M. H. The slow translation and rotation of two unequal spheres in a viscous fluid. *Chem. Eng. Sci.* **24,** 1769–1776 (1969).

Supplementary Information accompanies the paper on **www.nature.com/nature**.

Acknowledgements We thank E. Watson and Y. Inclán for technical assistance, E. Nogales for microscope time, and A. Vologodskii, V. Croquette, D. Bensimon, D. Collin, N. Pokala and Y. Chemla for critical readings of the manuscript and/or discussions. Z.B. is an HHMI predoctoral fellow, M.D.S. is supported by a PMMB training grant, and J.G. holds a fellowship from the Hertz Foundation. This work was supported by the NIH and DOE.

Competing interests statement The authors declare that they have no competing financial interests.

Correspondence and requests for materials should be addressed to C.B. (carlos@alice.berkeley.edu).

Visualization of an unstable coiled coil from the scallop myosin rod

Yu Li*†‡, Jerry H. Brown*, Ludmilla Reshetnikova*, Antal Blazsek§, László Farkas§, László Nyitray§ & Carolyn Cohen*

** Rosenstiel Basic Medical Sciences Research Center, and † Biophysics and Structural Biology Program, Brandeis University, Waltham, Massachusetts 02454-9110, USA*
§ Department of Biochemistry, Eötvös Loránd University, Pázmány P. s. 1/c, 1117 Budapest, Hungary

α-Helical coiled coils in muscle exemplify simplicity and economy of protein design: small variations in sequence lead to remarkable diversity in cellular functions[1,2]. Myosin II is the key protein in muscle contraction, and the molecule's two-chain α-helical coiled-coil rod region—towards the carboxy terminus of the heavy chain—has unusual structural and dynamic features. The amino-terminal subfragment-2 (S2) domains of the rods can swing out from the thick filament backbone at a hinge in the coiled coil, allowing the two myosin 'heads' and their motor domains to interact with actin and generate tension[3]. Most of the S2 rod appears to be a flexible coiled coil, but studies suggest that the structure at the N-terminal region is unstable[4–6], and unwinding or bending of the α-helices near the head–rod junction seems necessary for many of myosin's functional properties[7,8]. Here we show the physical basis of a

‡ Present address: Boston Biomedical Research Institute, 64 Grove Street, Watertown, Massachusetts 02472, USA.

particularly weak coiled-coil segment by determining the 2.5-Å-resolution crystal structure of a leucine-zipper-stabilized fragment of the scallop striated-muscle myosin rod adjacent to the head–rod junction. The N-terminal 14 residues are poorly ordered; the rest of the S2 segment forms a flexible coiled coil with poorly packed core residues. The unusual absence of interhelical salt bridges here exposes apolar core atoms to solvent.

The chimaeric peptide that we have crystallized (Fig. 1a) consists of Gly-Ser-His-Met at the N terminus, followed by residues 835–885 of the myosin heavy chain from the bay scallop *Argopecten irradians* (that is, the first 51 residues of the S2 domain, which we call 'S2N51'), a Gly-Ser linker, and residues 250–281 (the 'leucine zipper') of the yeast transcription factor GCN4 (see Methods). There are two independent 'molecular dimers' in the crystallographic asymmetric unit, each forming for the most part a parallel two-stranded α-helical coiled coil that is continuous through the Gly-Ser linker between S2N51 and GCN4. The two dimers follow somewhat different paths and seem to be flexible throughout their lengths (Fig. 1b), but their basic architectures are very similar. In each case there is increasing disorder from the C terminus to the N terminus. Along most of the relatively well-ordered C-terminal 63 residues of each chimaeric dimer, the interhelical distance is between 9 and 10 Å, typical of canonical two-stranded coiled coils. Closer to the N terminus (and further from the leucine zipper), from residues 857 to 849—where bulky methionine and glutamine residues are located in the core of the molecule—the crystallographic temperature factors rise and the diameter of the coiled coil increases to 11 Å. Another pair of poorly ordered helical turns occurs between residues 849 and 846 of each chain, and the N-terminal 8–11 residues of S2, as well as the N-terminal tetrapeptide of this construct, cannot be seen in the electron-density maps.

The structure of the core of scallop S2N51 reveals several features that seem to contribute to a flexible coiled coil (Figs 2 and 3). The key signature of α-helical coiled coils is a short-range seven-residue ('heptad') sequence repeat in the form 'abcdefg', where the core 'a' and 'd' residues are generally apolar. These residues form a left-handed apolar stripe along the surface of the right-handed α-helices, and their side chains interlock in a 'knobs-into-holes' fashion by the winding of helices around one another to produce the coiled-coil structure[1,2,9,10]. Scallop S2N51, despite the uninterrupted heptad repeat, has a large proportion of polar or charged residues in the core, especially at the N terminus. Here, the first three nominal 'd' positions of the sequence are occupied by a proline and two glutamine residues. Moreover, in each dimer of the asymmetric unit, the two 'd'-position Gln 849 residues pack in the core in an asymmetric fashion, with only one of the side chains forming a knob-into-hole contact with the opposite helix; the other side chain is oriented towards the solvent. (Asymmetrically packed glutamine residues also mark a boundary between coiled-coil and non-coiled-coil regions of tropomyosin[11].) These sequence features

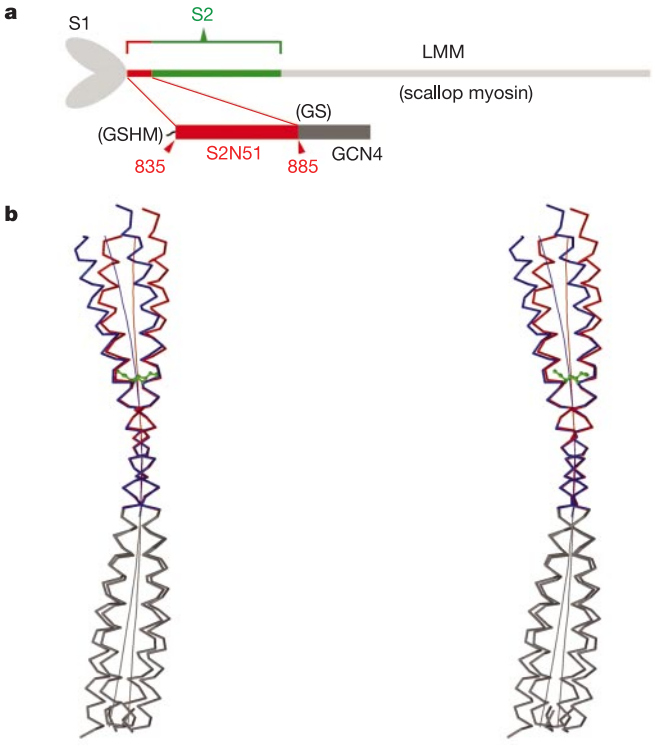

Figure 1 S2N51 is a flexible coiled coil. **a**, Diagrams of a myosin II dimer (top) and an expanded view of the construct crystallized in the present study (bottom). **b**, The two dimers of the crystallographic asymmetric unit are superimposed by fitting S2 residues 870–878 (S2N51 segments as red and blue Cα traces, shown in stereo). The structure near residue 867 (green) is particularly variable; here the coiled-coil axis (curved line) bends by only ~1° in one molecular dimer of the asymmetric unit (red) and by ~5° in the other (blue). Elsewhere along S2N51 both coiled coils bend by at least 3°. This continuous bending contrasts with the localized 'alanine' bending observed in tropomyosin[30] and the relative lack of bending (~2°) along the GCN4 portion of the dimer.

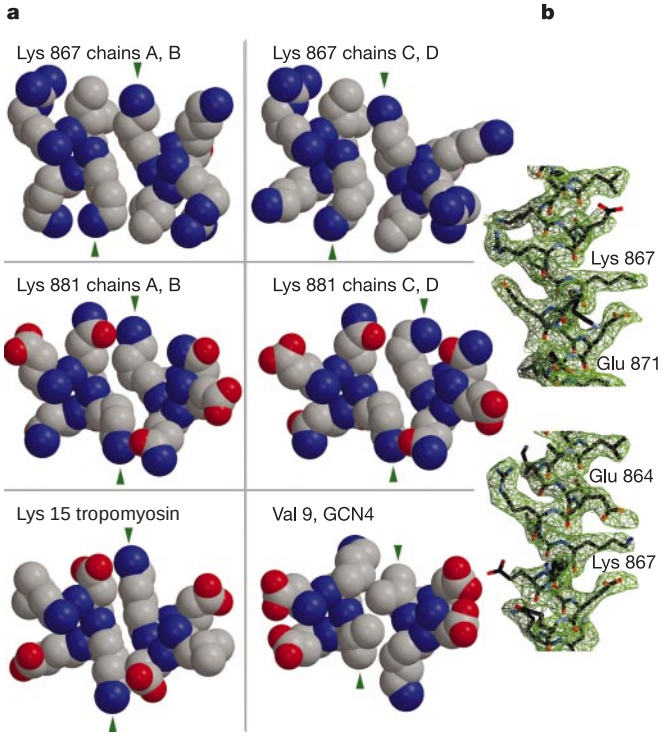

Figure 2 Scallop S2 displays non-close-packed regions in the core and conformationally variable 'a'-position lysine residues. **a**, In these views down the coiled-coil axis, green arrows point to the 'a' positions. In the top row (residues 865–869) and the middle row (residues 879–882) both dimers of the crystallographic asymmetric unit are displayed. The terminus of the Lys 867 side chain is generally oriented away from the core and from the unusual 'g'-position Ile 866, and instead interacts intrahelically with the 'e'-position glutamate residues 864 or 871 (shown in **b**) (see also Fig. 1b and the text). Lys 881 and Gln 880 form a core layer that is close packed only in one dimer of the asymmetric unit, where the lysine Cγ and Cδ atoms are puckered and nestle into the hole of the opposite helix. Also shown, for contrast, are a well-packed canonical knobs-into-holes 'a' layer of GCN4, and a 'g–a′' salt-bridge-stabilized layer of tropomyosin (bottom row). **b**, Region near Lys 867 in helix A (top) and helix D (bottom) viewed perpendicular to the axis. The $2|F_o|-|F_c|$ electron-density map is contoured at 1σ.

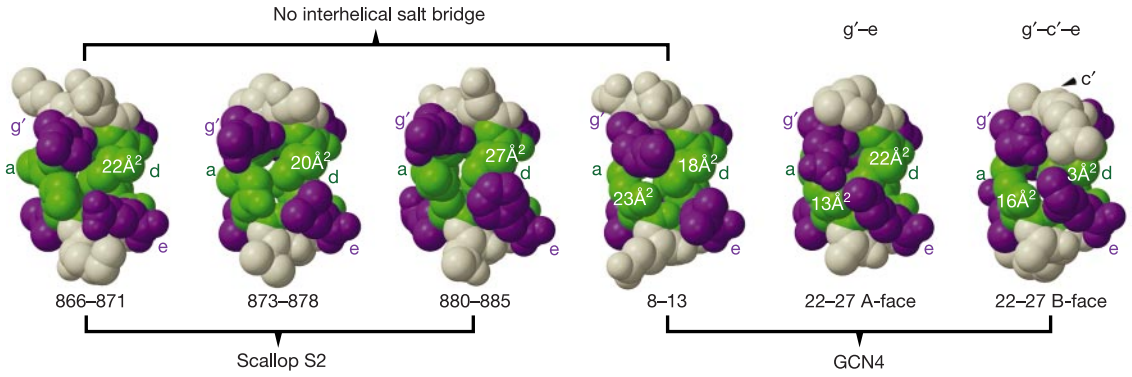

Figure 3 The absence of interhelical salt bridges between the 'g' and 'e' positions (purple) exposes core residues (green) to solvent. Each panel shows a horizontally oriented fragment of the coiled coil spanning heptad positions 'g', 'a', 'b', 'c', 'd' and 'e' from left to right. Solvent-accessible areas (in Å^2) calculated by SURFACE[31] are indicated for the apolar core residues (six 'd'-position leucines and three 'a'-position valines); other apolar core residues of S2N51 (not shown) are also highly exposed. Also note that depending on side-chain conformations, simple 'g–e′' salt bridges may bury either the intervening 'a' position (for example in the fifth panel) or the 'd'-position residue (for example leucine B39 of tropomyosin[30], solvent-accessible area 3 Å^2).

are consistent with the poor order in the density maps at the N-terminal 14 residues of scallop S2. In the remainder of scallop S2N51, 4 of the 10 core positions are polar (Fig. 4). The unbranched long lysine side chains in the 'a' positions 867 and 881 also adopt variable conformations, which form different sets of interhelical and intrahelical interactions on the surface of the coiled coil (see Fig. 2). Lys 867 is in fact adjacent to Ile 866, whose apolar and β-branched side chain is unusual for a 'g' position; these residues together form a poorly packed core for all four helices of the asymmetric unit (Fig. 2). Moreover, at this location the two molecules of the asymmetric unit follow distinctly different paths (Fig. 1b). (Note that a mutation from arginine to histidine at the corresponding position (870) of cardiac β-myosin is associated with familial hypertrophic cardiomyopathy[12]; because residue 867 is exposed in our structure and histidine is a less flexible side chain than arginine or lysine, we expect that this mutation might alter both the dynamic and interaction properties of the molecule.) The only canonical region in the core of S2N51 is near its C terminus, which contains three consecutive relatively conserved 'd'-position leucines (Fig. 4a) (but see below). As is found in other coiled-coil proteins, the canonical small or branched apolar core side chains can adopt only a few (generally two) rotamers and they consistently form interhelical knob-into-hole hydrophobic contacts, in contrast to the conformationally variable 'a'-position lysines.

Scallop S2N51 is also remarkable in lacking any interhelical salt bridges. Coiled coils seem to require intrahelical and interhelical salt bridges for their stability[13–15], especially those between the flanking 'e' and 'g' positions of neighbouring chains[16,17]. The first potential

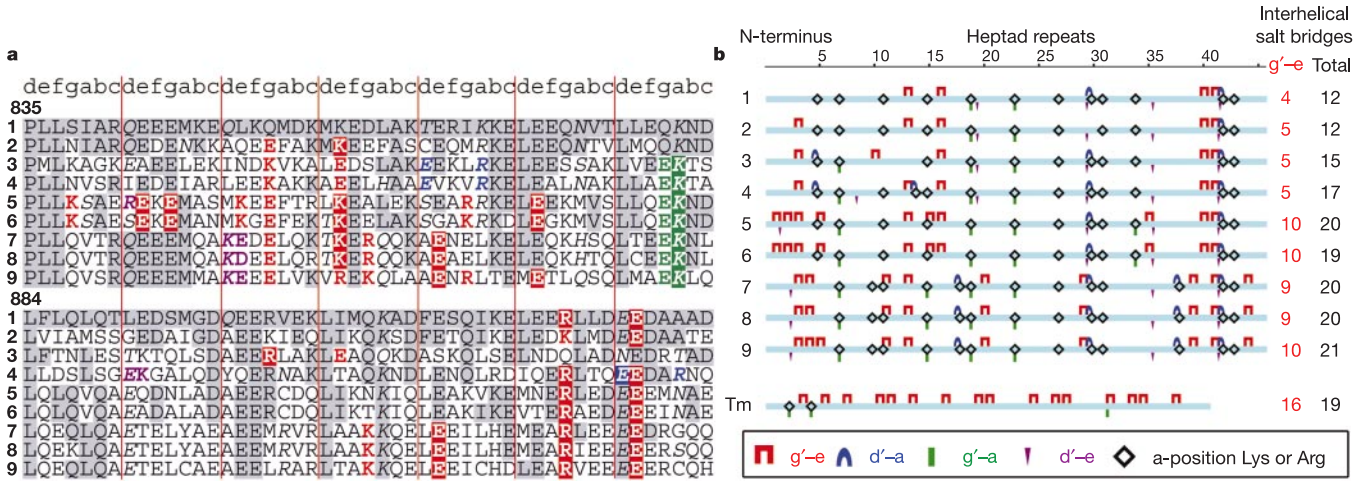

Figure 4 The N-terminal region of molluscan S2 (sequences 1 and 2) displays in an exaggerated way the moderately low level of coiled-coil-stabilizing features present in S2 of various myosins. The sequences of the N-terminal 14 heptads (**a**) and schematic summaries of S2 domains (**b**) from invertebrate (sequences 1–4), vertebrate striated muscle (sequences 5 and 6), vertebrate smooth muscle (sequences 7 and 8) and vertebrate non-muscle myosins II (sequence 9). The S2 sequences shown are from the striated adductor muscle of the bay scallop *Argopecten irradians* (GenBank accession no. 5612) (1), the ventral siphon of the squid *Loligo pealei* (GenBank 3252880) (2), the body wall muscle of *Caenorhabditis elegans* (unc-54, GenBank 17509401) (3), indirect flight muscle of *Drosophila melanogaster* (GenBank 20455497) (4), human cardiac muscle (β-myosin, GenBank 547966) (5), chicken (*Gallus gallus*) skeletal muscle (GenBank 6683485) (6), chicken-gizzard muscle (GenBank 86369) (7), human bladder and oesophagus muscles (GenBank 13432177) (8), and human platelet (GenBank 6166599) (9). For comparison, a schematic of the coiled coil of rat (*Rattus norvegicus*) striated-muscle α-tropomyosin (Tm) is also shown. In **a**, identities with the scallop sequence are shaded, core polar side chains (generally coiled-coil destabilizing) are italicized; in **b**, 'a'-position lysines and arginines are indicated by black diamonds, and in both panels the residues participating in interhelical 'g–a', 'd–e′', 'd–a' and the well-recognized[16,17] coiled-coil stabilizing 'g–e′' salt bridges are coloured green, magenta, blue and red, respectively.

interhelical salt bridge in scallop S2 occurs 88 residues from the head–rod junction, and the S2 regions of molluscan myosins have fewer potential interhelical salt bridges than do those of other conventional myosins (Fig. 4). (Note that this segment does have intrahelical salt bridges in numbers typical of other two-stranded coiled coils.) A comparison of the S2N51 structure with that of other coiled coils (Fig. 3) illustrates how 'g–e′' (and especially complex 'g–c–e′') salt bridges, in addition to providing ionic bonding between the two α-helices, can also contribute to the stability of a coiled coil by helping to bury residues in the core (see also ref. 17). The residues that are exposed in scallop S2N51 because of the lack of 'g–e′' links include the three consecutive 'd'-position leucines (Figs 3 and 4) as well as other apolar core side chains. Removal of apolar residues from aqueous solvent is a key driving force of protein folding, so that the stability of coiled coils might not simply be a function of the number of good (that is, apolar, leucine) 'a' and 'd' residues and the number of interhelical ('g–e′') salt bridges, but also of their specific locations relative to one another. The likely importance of the sequence context of charge pairs has been indicated by recent mutational studies of heterodimeric coiled coils[18]. A definite positional relationship in the primary sequence between locally clustered salt bridges and hydrophobic core residues is also a key feature of 'trigger sequences', which promote α-helical coiled-coil formation in several proteins[14].

The structure of the N-terminal 51 residues of S2 in scallop displays in an exaggerated way properties of the entire S2 domain. The sequences of S2 and the rest of the rod in diverse isoforms generally display somewhat fewer potential interhelical salt bridges (~0.3 per heptad)[19] and apolar residues in the core (~65%) as well as significantly more 'a'-position lysines and arginines (~20–25%)[20] than do most α-helical dimeric coiled coils[19–21] (see Fig. 4). Coiled-coil trigger sequences containing multiple potential salt bridges are also generally absent from the N-terminal region of S2. (In scallop S2 there is a trigger sequence[14] located 85 residues from the head–rod junction, but it is embedded in a region of poor coiled-coil potential.) Correspondingly, in contrast to particularly stable coiled coils with triggers such as those in cortexillin I (ref. 15) and the 33-residue GCN4 leucine zipper[10], relatively long N-terminal segments of S2 are often required for dimerization (more than 300 residues in scallop[6]). The extent of S2 instability seems to vary depending on the isoform[4–6,12].

Weakness in the N-terminal region of the S2 coiled coil seems to be an important aspect of its design. The disorder we have observed in the first heptad of the scallop structure is characteristic, in fact, of all conventional myosin isoforms, and is signalled by the conserved proline present at the head–rod junction. This structural feature accounts for the pivot needed for mobility of the head–rod junction. In all muscles, the S2 region must be strong enough to transmit tension efficiently during contraction, but localized weakness could contribute to the compliance of the myosin crossbridge. Mutational studies of chicken-gizzard myosin heavy meromyosin (HMM) indicate that instability at the head–rod junction might be important for optimal mechanical performance[7]. A locally weak dimeric S2 coiled coil might also be necessary to produce the 'off state' of regulated myosins. In myosins from vertebrate smooth muscles, regulation is controlled by the phosphorylation of a light chain in each of the heads of the molecule, whereas in myosins from scallop and other molluscan striated muscles control is effected by the direct binding of Ca^{2+} to the essential light chain[22]. The unphosphorylated off state of chicken smooth-muscle HMM and myosin has been visualized using cryoelectron microscopy of two-dimensional crystals: the molecules have a compact conformation with asymmetric interactions between the two heads[8]. By negative staining, the rod region has been shown to extend back from the S1–S2 junction and to run between the two heads[23]. This arrangement would appear to require an unwinding of perhaps one to two heptads of the coiled coil at the N terminus of S2. In scallop HMM, a similar compact conformation probably also occurs in the Ca^{2+}-free off states[24]. Note also that in scallop myosin, where the N-terminal region of S2 seems to be especially unstable[6], the time required for the 'switching on' of the heads is considerably shorter (within 10 ms (ref. 25)) than that for vertebrate smooth muscles. In contrast to these results on regulated myosins, it seems that the extent of instability in S2 is less in vertebrate skeletal-muscle myosin, because resonance-energy-transfer experiments indicate that in this S2, only the first heptad may be uncoiled when the two heads are bound to actin in the rigor state[26]. (In this regard, note the additional potential interhelical salt bridges near the N terminus of vertebrate skeletal S2 compared with regulated myosins (Fig. 4).) These various results use different methods, isoforms and states of contraction, but are beginning to yield crucial information to relate sequence to function.

A poorly stabilized coiled coil adjacent to the motor domains in the heads is a design that might also be used in kinesin (but see ref. 27) and in various unconventional myosins. Here, coiled-coil unwinding might help to account for otherwise puzzling properties of myosin VI, which—in contrast to conventional myosin II—has a short single IQ-repeat lever arm but is a processive two-headed motor with a large (possibly 36-nm) step size[28]. The N-terminal 60 residues of this coiled coil are also predicted to lack interhelical salt bridges. Taken together, these results bear out the versatility of the simple coiled-coil motif, which has both structural and dynamic roles in protein function[29]. □

Methods

For details of expression, purification, crystallization and structure determination, see Supplementary Methods. In brief, the chimaeric peptide (see Fig. 1a) was expressed in *Escherichia coli*, purified sequentially on nickel-affinity, MonoQ ion-exchange and Superdex 200 columns (Pharmacia), and was crystallized after repeated seedings at 16 °C against 15–20% poly(ethylene glycol) 2000 monomethyl ether, 50 mM NaCl, 2 mM NaN_3, 44 mM MOPS pH 6.9. X-ray data from a single crystal (cryopreserved with glycerol) were collected at 100 K ($P2_12_12_1$, $a = 54.04$ Å, $b = 73.30$ Å, $c = 102.97$ Å, 49% solvent). The structure was determined by a novel use of molecular replacement in which some conventional refinement was performed on a correctly oriented model before the calculation of the translation function (final $R_{free} = 0.286$ to 2.5 Å resolution; root-mean-square bond lengths and angles are 0.006 Å and 1.012°, respectively). Note that the GCN4 leucine zipper portion of the chimaeric peptide promotes the formation of the S2N51 coiled coil (otherwise transiently stable[6]) but is not expected to perturb its structure owing to the linear nature of the coiled-coil motif.

Received 6 January; accepted 20 May 2003; doi:10.1038/nature01801.

1. Cohen, C. & Parry, D. A. D. α-Helical coiled coils and bundles: How to design an α-helical protein. *Proteins* **7,** 1–15 (1990).
2. Lupas, A. Coiled coils: New structures and new functions. *Trends Biochem. Sci.* **21,** 375–382 (1996).
3. Huxley, H. E. The mechanism of muscular contraction. *Science* **164,** 1356–1365 (1969).
4. Trybus, K. M. Regulation of expressed truncated smooth muscle myosins. Role of the essential light chain and tail length. *J. Biol. Chem.* **269,** 20819–20822 (1994).
5. Knight, P. J. Dynamic behavior of the head–tail junction of myosin. *J. Mol. Biol.* **255,** 269–274 (1996).
6. Malnasi-Csizmadia, A., Shimony, E., Hegyi, G., Szent-Györgyi, A. G. & Nyitray, L. Dimerization of the head–rod junction of scallop myosin. *Biochem. Biophys. Res. Commun.* **252,** 595–601 (1998).
7. Lauzon, A. M., Fagnant, P. M., Warshaw, D. M. & Trybus, K. M. Coiled-coil unwinding at the smooth muscle myosin head–rod junction is required for optimal mechanical performance. *Biophys. J.* **80,** 1900–1904 (2001).
8. Liu, J., Wendt, T., Taylor, D. & Taylor, K. Refined model of the 10 S conformation of smooth muscle myosin by cryo-electron microscopy 3D image reconstruction. *J. Mol. Biol.* **329,** 963–972 (2003).
9. Crick, F. H. C. The packing of α helices: simple coiled-coils. *Acta Crystallogr.* **6,** 689–697 (1953).
10. O'Shea, E. K., Klemm, J. D., Kim, P. S. & Alber, T. X-ray structure of the GCN4 leucine zipper, a two-stranded, parallel coiled coil. *Science* **254,** 539–544 (1991).
11. Li, Y. *et al.* The crystal structure of the C-terminal fragment of striated-muscle α-tropomyosin reveals a key troponin T recognition site. *Proc. Natl Acad. Sci. USA* **99,** 7378–7383 (2002).
12. Gruen, M. & Gautel, M. Mutations in β-myosin S2 that cause familial hypertrophic cardiomyopathy (FHC) abolish the interaction with the regulatory domain of myosin-binding protein-C. *J. Mol. Biol.* **286,** 933–949 (1999).
13. McLachlan, A. D. & Stewart, M. Tropomyosin coiled-coil interactions: Evidence for an unstaggered structure. *J. Mol. Biol.* **98,** 293–304 (1975).
14. Kammerer, R. A. *et al.* An autonomous folding unit mediates the assembly of two-stranded coiled coils. *Proc. Natl Acad. Sci. USA* **95,** 13419–13424 (1998).
15. Burkhard, P., Kammerer, R. A., Steinmetz, M. O., Bourenkov, G. P. & Aebi, U. The coiled-coil trigger site of the rod domain of cortexillin I unveils a distinct network of interhelical and intrahelical salt bridges. *Structure* **8,** 223–230 (2000).
16. Meier, M., Lustig, A., Aebi, U. & Burkhard, P. Removing an interhelical salt bridge abolishes coiled-coil formation in a *de novo* designed peptide. *J. Struct. Biol.* **137,** 65–72 (2002).
17. Burkhard, P., Ivaninskii, S. & Lustig, A. Improving coiled-coil stability by optimizing ionic interactions. *J. Mol. Biol.* **318,** 901–910 (2002).

18. Arndt, K., Pelletier, J., Muller, K., Pluckthun, A. & Alber, T. Comparison of *in vivo* selection and rational design of heterodimeric coiled coils. *Structure* **10,** 1235–1248 (2002).
19. Conway, J. F. & Parry, D. A. D. Structural features in the heptad substructure and longer range repeats of two-stranded α-fibrous proteins. *Int. J. Biol. Macromol.* **12,** 328–334 (1990).
20. McLachlan, A. D. & Karn, J. Periodic features in the amino acid sequence of nematode myosin rod. *J. Mol. Biol.* **164,** 605–626 (1983).
21. Woolfson, D. N. & Alber, T. Predicting oligomerization states of coiled coils. *Protein Sci.* **4,** 1596–1607 (1995).
22. Adelstein, R. S. & Eisenberg, E. Regulation and kinetics of the actin–myosin–ATP interaction. *Annu. Rev. Biochem.* **49,** 921–956 (1980).
23. Burgess S. *et al.* Structure of smooth muscle myosin in the switched-off state. *Biophys. J.* (annual meeting abstracts), 356a (2002).
24. Stafford, W. F. *et al.* Calcium-dependent structural changes in scallop heavy meromyosin. *J. Mol. Biol.* **307,** 137–147 (2001).
25. Nyitrai, M., Szent-Györgyi, A. G. & Geeves, M. A. A kinetic model of the co-operative binding of calcium and ADP to scallop (*Argopecten irradians*) heavy meromyosin. *Biochem. J.* **365,** 19–30 (2002).
26. Chakrabarty, T., Xiao, M., Cooke, R. & Selvin, P. R. Holding two heads together: Stability of the myosin II rod measured by resonance energy transfer between the heads. *Proc. Natl Acad. Sci. USA* **99,** 6011–6016 (2002).
27. Tomishige, M. & Vale, R. D. Controlling kinesin by reversible disulfide cross-linking. Identifying the motility-producing conformational change. *J. Cell Biol.* **151,** 1081–1092 (2000).
28. Buss, F., Luzio, J. P. & Kendrick-Jones, J. Myosin VI, a new force in clathrin mediated endocytosis. *FEBS Lett.* **508,** 295–299 (2001).
29. Burkhard, P., Stetefeld, J. & Strelkov, S. V. Coiled coils: A highly versatile protein folding motif. *Trends Cell Biol.* **11,** 82–88 (2001).
30. Brown, J. H. *et al.* Deciphering the design of the tropomyosin molecule. *Proc. Natl Acad. Sci. USA* **98,** 8496–8501 (2001).
31. Collaborative Computational Project, Number 4. *Acta Crystallogr. D* **50,** 760–763 (1994).

Supplementary Information accompanies the paper on **www.nature.com/nature**.

Acknowledgements We thank D. A. D. Parry, A. G. Szent-Györgyi and H. E. Huxley for a critical reading of the manuscript, and the staff of the Cornell High Energy Synchrotron Source for assistance with data collection. This work has been supported by grants to C.C. from the National Institutes of Health and the Muscular Dystrophy Association, and to L.N. from the Hungarian Scientific Research Fund (OTKA).

Competing interests statement The authors declare that they have no competing financial interests.

Correspondence should be addressed to (ccohen@brandeis.edu). X-ray coordinates have been deposited at the Protein Data Bank, Brookhaven (1NKN).